CHEMISTRY OF MATERIALS

Article

Cite This: Chem. Mater. 2014, 26, 6142-6151

pubs.acs.org/cm

Carboxyl Group Enhanced CO Tolerant GO Supported Pt Catalysts: DFT and Electrochemical Analysis

S. Sharma,*[,†] M. N. Groves,[§,¶] J. Fennell,[‡] N. Soin,[∥] S. L. Horswell,[‡] and C. Malardier-Jugroot[§]

[†]Centre for Hydrogen and Fuel cell Research, School of Chemical Engineering, University of Birmingham, Edgbaston, Birmingham B15 2TT, United Kingdom

[§]Department of Chemistry and Chemical Engineering, Royal Military College of Canada, Kingston, Ontario K7K 7B4, Canada

[‡]School of Chemistry, University of Birmingham, Edgbaston, Birmingham B15 2TT, United Kingdom

[∥]Institute for Renewable Energy and Environmental Technologies (IREET), Knowledge Centre for Materials Chemistry (KCMC), University of Bolton, Bolton BL3 5AB, United Kingdom

Supporting Information

ABSTRACT: The effect of residual oxygen species in as-prepared Pt nanoparticle on partially reduced graphene oxide (Pt/PRGO) and partially reduced carboxylated-GO (Pt/PR(GO−COOH)) supports was investigated using electrochemical CO stripping and density functional theory (DFT) analysis. Pt/PRGO and Pt/PR(GO−COOH) revealed a clear negative shift in CO-stripping onset potential compared to commercial Pt/carbon black. DFT analysis confirmed that the presence of a −COOH group provides the most resistance for CO adsorption. This CO-Pt binding energy is significantly lower than that observed in the presence of an −OH group, which is the most abundant oxygen group in carbon supports. The Pt-CO dissociation energies (on a 42-atom graphene sheet) in the presence of various oxygen groups, in descending order, were OH > C═O ≈ C−O−C > COOH. Although single-bonded carbon−oxygen groups (−OH and C−O−C) are more abundant on the GO basal plane and play an important role in Pt nanoparticle nucleation and distribution on graphene sheets, the double-bonded carbon−oxygen (C═O and COOH) groups are more abundant residual species post Pt nanoparticle growth and play a vital role in enhancing CO tolerance.

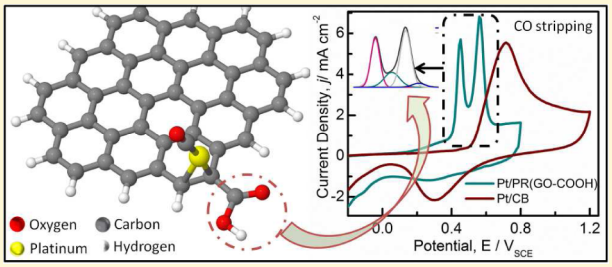

INTRODUCTION

Platinum (Pt) has long been used as one of the most efficient catalysts for a wide range of applications including low temperature acid and alkaline-based fuel cell systems,[1−3] electrolyzers,[4,5] hydrogen purification,[6−10] and other catalytic reactions such as hydrogenation of hydrocarbons.[11−15] However, the vulnerability of Pt nanoparticles toward carbon monoxide (CO) poisoning is a major drawback affecting the efficiency and the long-term performance of catalysts in all these applications. An enhancement in the CO tolerance of the Pt electrocatalysts for the aforementioned applications would result in the following: (a) the low-temperature fuel cell systems would not require ultrapure hydrogen, and the process of hydrogen purification will become more efficient thereby reducing the existing costs significantly; (b) higher concentration of methanol or ethanol can be used in alcohol-based fuel cells allowing higher current and output power along with enhanced durability; (c) hydrogenation of hydrocarbon would become more effective and economical; and most importantly, (d) increased efficiency of Pt catalyst would mean reduced dependence on this rare and limited resource. Currently, the most effective way of increasing CO tolerance is the use of oxophilic elements such as Ru, Pd, Au, and so forth, to form alloys with Pt.[16−19] However, this is an extremely costly solution as all these elements (like Pt) are in limited supply and hence quite expensive. It is, therefore, essential to investigate other cheaper alternatives such as surface modification and functionalization of the underlying support to provide synergistic effects for enhancing the CO-tolerance of Pt.

With the rise of graphene and graphene-based materials, the use of reduced and/or partially reduced graphene oxide (PRGO) as catalyst support for Pt and Pt-based alloy as catalysts for direct methanol (DMFC) and polymer electrolyte membrane (PEMFC) fuel cells,[20−22] hydrogenation,[23] and hydrogen -storage systems[24,25] applications has been investigated intensively in the past few years. In many applications such as catalyst−support systems, polymer−graphene conjugates, the defects introduced in the graphene structure due to the introduced oxygen groups make PRGO much more suitable, as compared to the expensive to synthesize, defect-free graphene. The defects in PRGO are created by the initial heavy oxidation of graphite to produce graphene oxide, GO

Received: July 5, 2014
Revised: October 10, 2014
Published: October 11, 2014

   dx.doi.org/10.1021/cm502447s | Chem. Mater. 2014, 26, 6142−6151

(via Hummer's method) and then further enhanced by the loss of CO_2 during the reduction process. These defects provide ideal sites for nanoparticle nucleation and growth. Recent studies on DMFC applications have also revealed that the residual oxygen species on the reduced or partially reduced graphene support seem to play a crucial role not only in improving the catalyst−support interaction and the catalyst adhesion on the support but also in enabling a narrow particle size distribution and most in enhancing the CO-tolerance of the Pt catalyst.[20,21,26,27] Density functional theory (DFT) studies have supported these reports by suggesting that the high binding energy between Pt clusters and the unreconstructed defects in reduced graphene oxide lead to a shift in the Pt cluster d-band center even below that of Pt (111) facilitating enhanced CO-tolerance.[28] On the other hand, DFT studies on doped graphene systems have suggested that oxygen-doped graphene showed the highest binding energy (7-fold higher than undoped graphene) with Pt atoms, as compared to other dopants such as nitrogen, boron, and beryllium.[29] However, there are a variety of oxygen functional groups (hydroxyl, carboxyl, carbonyl, epoxy) that are present on an oxygen-functionalized graphene sheet or PRGO supporting Pt nanoparticles. Consequently, Pt nanoparticles supported on the PRGO (Pt/PRGO) are known to have a considerable number of oxygen groups in their vicinity.[20,26] These oxygen functional groups create a complex surrounding around each Pt nanoparticle, which could possibly generate a special micro-environment in the presence of an approaching CO molecule. At this point, it is essential to point out that graphene oxide (GO) is an extremely heterogeneous material (consisting of randomly distributed domains of sp^2 and sp^3 hybridized carbons)[30,31]whose initial oxidation level, as well as the distribution of the variety of oxygen groups (−OH, C−O−C, −C═O, COOH), will not only depend on the macro-oxidation conditions like time, temperature and concentration of the oxidizing agents used, but also on the micro-conditions such as sheet/particle size of graphite used and intrinsic local defects in the initial graphite structure. Consequently, post-oxidation and reduction steps significantly affect the distribution of the residual oxygen groups in the PRGO system. All this will in turn affect the local micro-environment around an individual Pt nanoparticle and govern its response toward an approaching CO molecule. It is, therefore, critical to examine in great detail how the Pt/PRGO system interacts with an approaching CO molecule, and given the large complexities of the GO and the resulting PRGO structure, how each of these oxygen species elicits a different response. A study of how the different oxygen functional groups affect the Pt−CO interaction independently as well as in combination with other functional groups would help understand the different micro-environments that are present in these catalyst−support systems and how these affect the Pt−CO interaction in Pt/PRGO systems.

This work studies the effects of various residual oxygen groups in PRGO toward Pt−CO interaction by combining DFT analysis with electrochemical CO stripping. DFT studies revealed that a graphene sheet with a −COOH group near the Pt atom in particular enabled a much higher resistance to CO adsorption; as such, the effect of the presence of excess −COOH (by using partially reduced carboxylated GO or PR(GO−COOH) system) was investigated in further detail using electrochemical analysis to support DFT studies. These studies could be very helpful in understanding and tailoring the environment around Pt nanoparticles (as well as other metal nanoparticles) on the PRGO support to achieve enhanced CO tolerance and improved catalyst efficiencies. To the best of our knowledge, no studies so far have ever looked into the complex PRGO system to examine the effect of its various oxygen functional groups on Pt−CO interactions.

EXPERIMENTAL SECTION

Synthesis of Graphene Oxide and Carboxylated Graphene Oxide. All chemicals (analytical grade) were purchased from Sigma-Aldrich and were used without any further purification steps. Graphene oxide (GO) was synthesized using a modified Hummer's oxidation process, which is described in detail elsewhere.[32,33] Using the as-prepared GO, carboxylated graphene oxide (GO−COOH) was synthesized using NaOH and $CH_2ClCOONa$. Typically, 10 g of NaOH and 10 g of $CH_2ClCOONa$ were mixed with 200 mL of 1 mg/mL solution of GO and ultrasonicated for 2 h to convert hydroxyl and epoxide groups into carboxyl groups. The mixture was then neutralized with 300 mL of 1 M HCl and was further washed extensively with copious amounts of water by filtration. The solid black product obtained was further purified by dialysis for 48−72 h to remove any residual Na or Cl ions, after which the samples were dried in a vacuum oven at 40 °C.[34]

Synthesis of Pt/PRGO and Pt/PR(GO−COOH). To synthesize Pt nanoparticles on the partially reduced GO and GO−COOH, a typical microwave-assisted polyol process was employed to achieve 25 wt % loading for both Pt/PRGO and Pt/PR(GO−COOH). For the Pt/PRGO synthesis, the process is detailed elsewhere.[20] For Pt/PR(GO−COOH), the same procedure was followed by simply replacing GO with GO−COOH. Further details can be found in the Supporting Information.

Material Characterization. The as-prepared GO, GO−COOH, Pt/PRGO, and Pt/PR(GO−COOH) were all characterized using X-ray photoelectron spectroscopy (XPS) using an Al Kα ($h\nu$ = 1486.6 eV) source, thermogravimetric analysis (TGA) was carried out on an SDT 2960 simultaneous DTA−TGA instrument (TA Instruments) from room temperature to 900 °C at heating rate of 10 °C/min in air, flowing at 100 mL/min. The X-ray diffraction analysis of the samples was carried out on Bruker D2, employing a Co Kα source. Transmission electron microscopy (TEM) was carried on a Tecnai TF20 instrument, operating at 200 kV. For comparison purposes, all studies and characterizations were also carried out on commercially available 46 wt % platinum nanoparticles supported on carbon black (Alfa-Aesar).

Catalyst Ink and Electrode Preparation for CO-Stripping. Water used throughout was purified with a Millipore A10 system (Millipore, France, resistivity >18 MΩ cm, toc ≤5 ppb). Catalyst inks of Pt/PRGO and Pt/PR(GO−COOH) were prepared keeping in mind the metal loading determined using TGA to prepare 10 $\mu g/cm^2$ of Pt loading on the working electrode. Appropriate amounts of water, iso-propyl alcohol, and nafion were mixed along with the Pt/PRGO or Pt/PR(GO−COOH) as required and ultrasonicated to obtain a uniform dispersion. For the working electrode, a 2 mm diameter glassy carbon electrode (GCE) was polished using alumina slurries of successively finer grains of alumina (1.0 μm, 0.3 μm, 0.05 μm) and rinsed thoroughly with ultrapure water to remove any traces of alumina. 20 μL of the as-prepared inks were then drop dried on the GCE.

Electrochemical Measurements. A standard three-electrode setup was completed using Pt as the counter electrode and saturated calomel electrode (SCE) as the reference electrode. All potentials in this work will be reported w.r.t. SCE. All glassware was cleaned by heating in a 1:1 mixture of concentrated nitric and sulfuric acids for 1 h, followed by rinsing with copious amounts of ultrapure water and soaking in ultrapure water overnight. For CO-stripping experiments, 0.1 M $HClO_4$ was used as the electrolyte and was purged initially with Ar to remove any oxygen or air from the solution. The electrolyte solution was then saturated with CO by bubbling CO for 15 min through the solution. The working electrode was held at 0.055 V for 5 min to enable CO adsorption, and subsequently, the solution was

dx.doi.org/10.1021/cm502447s | Chem. Mater. 2014, 26, 6142−6151

purged with Ar to remove any unadsorbed CO from the solution. CO stripping was performed using a cyclic voltammogram in the potential window from −0.25 to 1.25 V (vs SCE) at a scan rate of 50 mV/s. All cyclic voltammetry measurements in CO-free solution were performed with a CHI601B potentiostat (CH Instruments), and CO-stripping measurements were carried out with an Autolab PGStat12 controlled with GPES software.

RESULTS AND DISCUSSION

CO-Stripping Studies for Pt/PRGO and Pt/CB on GCE. Figure 1a shows the CO-stripping peaks observed for three Pt/PRGO samples and standard commercial Pt/CB normalized to their respective Pt loadings (see Supporting Information for complete CV scans). The voltammograms shown in Figure 1a consists of three scans of Pt/PRGO and two scans of Pt/CB showing the repeatability in the sample response toward the CO stripping. The scans clearly show that the CO-stripping charge for Pt/CB is much higher (up to 6 times higher than the area of the CO-stripping peak for Pt/PRGO), which is indicative of the fact that the Pt/CB is more susceptible to CO adsorption, whereas the Pt/PRGO system is relatively more resistive or tolerant toward adsorption of CO. CO-stripping scans for Pt/PRGO samples revealed broad and complex peaks in the potential window from 0.36 to 0.7 V. The onset potential for CO stripping for Pt/PRGO samples lies between 0.36 and 0.4 V, although for Pt/CB samples, it lies between 0.45 and 0.5 V. The lower or more negative onset potential for Pt/PRGO clearly suggests that the PRGO support weakens the Pt-CO interaction enabling an easier and quicker release of CO_{ads} from the Pt catalytic site and thereby leaving the Pt catalytic sites available for further reactions. At this point, it is essential to point out that the particle size distribution and crystal facets of Pt nanoparticles are very similar (3−5 nm) in Pt/CB and Pt/PRGO systems (as observed in the XRD and TEM data), and hence, these aspects are not expected to contribute significantly to the observed changes in the onset potential.

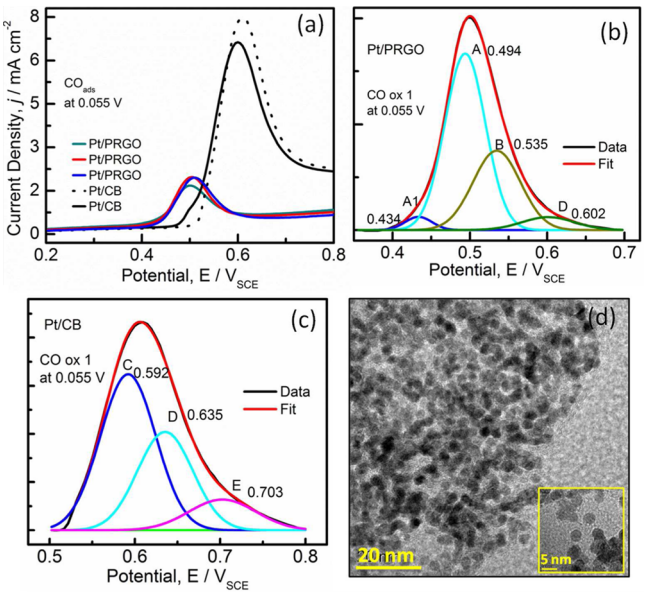

Figure 1. (a) Comparison of CO-stripping peaks obtained for Pt/PRGO and Pt/CB; deconvolutions of CO-stripping voltammograms for (b) Pt/PRGO and (c) Pt/CB; (d) TEM image of Pt/RGO.

The Pt/PRGO CO-stripping scans revealed a peak centered around 0.5 V, with possible components occurring as shoulders to the main peak (Figure 1b). Previous studies reporting on the CO-stripping for Pt and PtRu supported on highly reduced graphene oxide (where almost all the oxygen species were removed in the process of reduction; however, no information was provided regarding C/O ratio in the reduced GO) show a sharp CO oxidation peak close to 0.8 V_{RHE} (i.e., ∼0.56 V_{SCE}).[27,35] Meanwhile, the Pt/CB CO-stripping scans show a relatively sharp peak at 0.6 V with a shoulder close to 0.5 V. The peak potentials observed (0.6 vs SCE) for our Pt/CB samples are similar to those reported by other groups for Pt/CB. Table S4 displays a compilation of the CO-stripping peaks reported in the literature for bulk and nanocrystalline Pt on various carbon substrates. Broad CO-stripping peaks with multiple components have often been reported for PtRu alloys systems and have previously been attributed to the catalyst inhomogeneities, such as possible presence of mixtures of PtRu alloy along with Pt oxides and Ru oxides.[36−38] However, few attempts have been reported to identify the various elements or peak components for such broad peaks. Nevertheless, the similarity of the observations reported in the present work with those reported previously for PtRu alloys suggest that the oxidized GO support may exhibit a mechanism similar to that seen for Ru and other oxophilic materials toward CO oxidation. This has also been suggested in a previous report by Sharma et al.[20]

To further understand the nature of CO stripping, the Pt/PRGO CO-stripping peaks were deconvoluted to reveal three to four components, located at 0.42, 0.47, 0.53, 0.58, and 0.61 V, respectively (Figure 1b, c). The details of the peak fitting can be found in the Supporting Information. Deconvolutions were also carried out for Pt/CB peaks revealing up to three components at 0.59, 0.63, and 0.70 V, respectively. For Pt/PRGO samples, due to the inherent inhomogeneity of the distribution of chemical groups (as discussed earlier), some changes in the area under the peaks could be observed; however, the peak positions were consistent to ±0.01 V for all the measured samples. Pt/CB samples on the other hand, did not show any shifts in peak position or change in area under the peak. For comparison purposes, the various peak components (whose position was identified based on literature data and DFT studies in this work) observed have been labeled as A1 (0.41−0.44 V), A (0.47−0.49 V), B (0.53−0.55 V), C (0.57−0.59 V), D (0.60−0.61 V), and E (0.66−71 V) throughout the rest of this communication. As mentioned above, for Pt/PRGO samples, while the positions of the various peaks were consistent, the contribution of each component to the resultant CO-stripping peak varied from sample to sample. Because the graphite undergoes a very strong oxidation and acid treatment followed by acid and water cleaning during the GO synthesis by Hummers oxidation process, any impurities are expected to have been removed. Moreover, no other alloying elements or impurities were found in the samples during XPS analysis. Hence, the presence of these multiple components with variable contributions suggests the presence of differing combinations of residual oxygen groups on the graphene sheet leading to multiple micro-environments.

The CO-stripping data for Pt/PRGO samples, revealed multiple peaks from A1 (0.41−0.44 V), A (0.47−0.49 V), B (0.53−0.55 V), and D (0.60−0.61 V) with the main peak at 0.5 V. Interestingly, the CO-stripping data for the Pt/CB sample (Figure 1b) revealed no more than three components C (0.57−0.59 V), D (0.60−0.61 V), and E (0.66−71 V) in the potential window from 0.4 to 0.8 V with the main peak

dx.doi.org/10.1021/cm502447s | Chem. Mater. 2014, 26, 6142−6151

occurring at 0.6 V. The clear shift in the active potential window to more positive potentials for Pt/CB indicates the overall higher Pt−CO interaction energies for the Pt/CB system compared to the Pt/PRGO system. The presence of the other low-potential peaks in the GO-based support hints at the complex interaction taking place between the approaching/adsorbed CO molecule and the various oxygen groups in the vicinity of the target Pt nanoparticle. For Pt/CB, the peak D (centered at ∼0.6 V) is commonly observed for CO oxidation for carbon-supported Pt nanoparticles and is attributed to the CO oxidation occurring at isolated nanoparticles.[39] The term "isolated nanoparticles" generally refers to nanoparticles with no other nanoparticles nearby for available electron/charge transfer. However, the most striking feature is that the contribution of this Pt−CO (∼0.61 V) component in the Pt/PRGO CO-stripping peak is much smaller than that of the sharp peak (centered at 0.6 V) observed in the deconvoluted peak of Pt/CB. This means that more CO oxidation is occurring at isolated Pt nanoparticles in Pt/CB, as compared to Pt/PRGO, suggesting the presence of more isolated Pt nanoparticles in Pt/CB. This could be due to the porous microstructure of CB. However, because the loading in the Pt/CB system is high (46.9 wt %) compared to Pt/PRGO (25 wt %) it seems quite unlikely that more Pt nanoparticles are isolated in Pt/CB than Pt/PRGO. Previous studies suggest that the presence of residual oxygen functional groups in the vicinity of Pt nanoparticles in Pt/PRGO enables a d-band shift (similar to that seen in Pt-alloy systems) that leads to increased CO tolerance.[28] This resistance to CO adsorption was further confirmed by DFT analysis, which has been discussed further in this work. Consequently, even when the particles are isolated (from other Pt nanoparticles), the synergistic response from a PRGO support leads to a quicker $CO-CO_2$ conversion and release, most probably following the Mars van Krevlin mechanism, leading to a negative-shift toward lower stripping potentials. Hence, any isolated Pt nanoparticles on PRGO are never isolated from the residual oxygen groups, suggesting thereby that PRGO is a more active support compared to CB. Because the Pt/CB sample has a high Pt loading of 46.9 wt %, the component "A" can be associated with interparticle oxidation occurring due to close proximity of $-OH_{ads}$ and $-CO_{ads}$ species in aggregated conditions.[39] However, a similar peak has also been observed at Pt (111) crystallographic planes.[40] Because Pt (111) facets are the most abundant lattice sites observed commonly on Pt nanoparticles nucleating on carbon supports[20,21] (also see XRD in Figure S1), the possibility of interparticle oxidation occurring at Pt (111) sites due to generation of (aggregation led) terrace-like features[41] cannot be excluded.

For the Pt/PRGO system, the peak "A", similar to Pt/CB, can again be attributed to the interparticle oxidation. Although the Pt loading in this system was only 25 wt % and the TEM images confirm the absence of any aggregations, interparticle oxidation may well be facilitated by the presence of well-known C−C bond stretching, rippling, and sheet-folding features in graphene oxide sheets decorated with oxygen groups,[42] which can in turn give rise to specific spatial orientations (similar to terrace or step features) favorable for interparticle oxidation. The presence of oxygen functional groups like −COOH and C−O−C/C═O may also simulate similar spatial conditions. The peak "C" has been previously reported for Pt nanoparticles (30−50 wt %) on carbon support.[39] The Pt/PRGO peak "B" and the small Pt/CB component "E" (at 0.7 V) is not reported in the literature. However, DFT studies (discussed later) revealed that the Pt−CO dissociation energy in the presence of −OH group was found to be the highest, even higher than the dissociation energy of Pt-CO on graphene with no functional groups. Keeping this in mind, along with the well-known fact that the only known oxygen groups in CB are −OH groups;[32] the component peak at higher potential of 0.7 V may be attributed to the presence of −OH groups.

Density Functional Theory (DFT) Simulations. To understand the CO-stripping peak components and their relation to the complex PRGO structure, DFT was used to examine the individual effect of each functional group on the CO-Pt binding energy. The reference system composed of a Pt atom situated in the center site of a 42-atom hydrogen terminated graphene sheet with CO adsorbed onto it. The one-atom Pt configuration was chosen for the DFT simulation to characterize the Pt-CO interaction without the influence of different Pt-surface effects or nanocluster edge effects. Given the nature of the various GO groups, two cases, one where the Pt is adsorbed on the center of the sheet and the other when it is adsorbed on the edge of the sheet, were investigated.

The center of the sheet reference system is composed of a Pt atom bridged over the two centre carbon atoms in a 42-atom hydrogen terminated graphene sheet with CO adsorbed onto it. As in all cases, when the CO molecule was added, it was placed 2.0 Å above the Pt atom, vertically aligned with the carbon atom facing down and then relaxed. The binding energy of the CO to the Pt in this case was calculated to be −2.88 eV. This value is much higher than the experimentally determined adsorption energy range of 1.41−1.43 eV measured at a low coverage of CO on a Pt (111) surface.[43a,b] It is, however, not unexpected to calculate a larger adsorption energy for CO adsorbed onto very small Pt clusters[43c] and Pt clusters supported by graphene sheet.[43d] In the second case, the edge case, the Pt atom is instead adsorbed at an edge site bridged between two carbons terminated with hydrogen atoms. This system is calculated to be 0.91 eV more stable than when the Pt is adsorbed on the center of the sheet. When CO is added to this system, it adsorbs onto the Pt with a binding energy of −2.42 eV. Based on these values, it is clear that the Pt would tend to localize on edge sites and that this lowers the CO−Pt binding energy. This second case is an attempt to infer the effects of defects based on the proximity of adsorbates to the edge of the graphene sheet (see details in Table S1). Moreover, the position of the defects, their distribution, and the distribution of the functional groups were not experimentally controlled and it would be therefore very difficult to obtain a trend, which could be linked directly to the electrochemical analysis. These two cases were used as reference to discuss the influence of a given GO functional group on the binding energy (enhanced or weakened), which in turn indicates greater or lesser extent of adsorption and/or more facile removal of CO from Pt.

Several configurations were tested, and the lowest energy case of each was used for comparison. Given that the operating temperature for the applications of these catalyst layers are at least at room temperature, it was assumed that they will all have the opportunity to relax into these low-energy states. According to our results, the low energy states with CO are consistent with the corresponding configuration without CO. The only exception was in the carbon−oxygen double-bond (C═O) case. This will be discussed in detail in the following sections. For three of the cases, the average, highest binding energy, and

dx.doi.org/10.1021/cm502447s | Chem. Mater. 2014, 26, 6142−6151

lowest binding energy configurations tested are also reported to provide insight into the range of binding energy values that are present in the system. Although the Pt−CO binding energy from the complex which relaxes to the lowest energy will be the primary indicator for which a system resists CO adsorption the most, the stability of the system prior to and after CO adsorption must also be considered given that it must be likely for a state to be present in order to reliably benefit from its calculated effect.

It is known that the hydroxyl groups (present on the carbon support) bind strongly to Pt and inhibit other reactions from occurring on fuel cell electrodes.[44] To determine their effect on the CO-Pt interaction, a graphene flake with a Pt atom above its center was relaxed and then optimized again with an −OH group placed at six unique locations around the Pt on the graphene sheet. This was to determine the initial condition of the system prior to the addition of CO molecule. In every case, except one, the −OH group migrated and bonded to the platinum atom preventing the CO from adsorbing onto it. In one case where the −OH group did not bond to the Pt, the CO was adsorbed instead and the CO-Pt binding energy was calculated to be −3.12 eV (Figure 2b). This migration of the

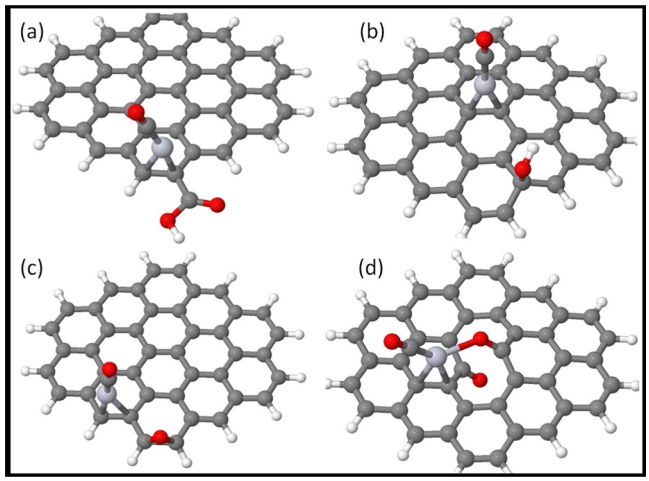

Figure 2. Pt−CO interaction in the presence of the different oxygen groups with the most stable configuration for each oxygen functional group with carbon in gray, hydrogen in white, oxygen in red, and platinum in light gray: (a) COOH functional group; (b) hydroxyl (−OH) functional group; (c) bridging oxygen (C−O−C) functional group; (d) carbonyl (>C═O) functional group.

OH group to bind to Pt does prevent CO poisoning, given that the −OH is considered a spectator species;[44−46] however, it does not help the Pt accomplish its role as a catalyst. Hence, the −OH groups do not seem to be a beneficial species in terms of preventing CO poisoning of the platinum catalyst.

The carbon−oxygen double-bond system (carbonyl, >C═O) was composed of two C═O groups in the center of the sheet in order to ensure that no dangling bonds existed. Hydrogen was not used in order to prevent it from becoming part of the interaction. The two C═O groups were set in sheet and the Pt atom was instead positioned at 14 sites over one-half of the sheet. It is assumed that the symmetry of the sheet only acts along the long axis so more sites were examined in this case. Several duplicate systems were found once the 14 initial platinum sites were relaxed. Six unique configurations remained for CO addition. The lowest energy state with the CO molecule is shown in Figure 2d. The most stable CO binding energy was calculated to be −2.58 eV. This value represents a significant decrease from that calculated for the plain graphene sheet. What is interesting to note is that for the C═O system, one of the cases was found to have a binding energy of −2.08 eV. This low binding energy state also corresponds to the configuration with the lowest energy state without CO adsorbed on to the Pt. Furthermore, these two sites are also adjacent to each other in terms of Pt adsorption on the graphene flake. This suggests that when the CO is adsorbed onto the Pt, it resides in the configuration shown in Figure 2d with a binding energy of −2.58 eV. However, given its proximity to the second, low binding energy state (−2.08 eV), what may have also been found is an intermediate for CO desorption or turning the CO into CO_2 according to the Mars−van Krevelin reaction mechanism[47,48] using the C═O surface group.

For the bridged oxygen system (epoxide, C−O−C), the Pt atom was initially located in the center of the graphene sheet. The oxygen atom was then located in 11 bridge positions over one-quarter of the sheet assuming that the symmetry of the sheet would yield similar results if the oxygen were placed in any of the other three-quarters. Through this search, it was found that it was more favorable for the oxygen to bridge carbon atoms at the edge of the sheet over the ones closer to the center where the Pt atom was located. Using the most stable location for the bridged oxygen atom, three new locations for the Pt atom were calculated. They were also located close to or at the edge of the sheet in sites that are once removed from being adjacent to the oxygen. Consistent with the reported reference results above, a more stable position was found with the Pt at an edge site next to the oxygen. The CO molecule was added to each of the 14 cases examined. The most stable configuration was the same edge site as when the CO molecule was not present and is illustrated in Figure 2c. This will be the site used to compare against the other graphene oxide types for CO binding energy, and it was calculated to be −2.54 eV. The lowest binding energy case for the C−O−C functional group corresponds to an additional calculation where the positions of the oxygen and Pt atoms illustrated in Figure 2c are exchanged. The CO−Pt binding energy in this case is −2.33 eV. However, this exchanged configuration of Pt and C−O−C on the graphene sheet is 0.19 eV less stable than the original configuration illustrated in Figure 2c without CO present, and 0.41 eV less stable when CO is present. Even though there is a reduction in the Pt−CO binding energy when the Pt is adsorbed onto that specific edge site bridged over two carbons terminated by hydrogen atoms, it is thermodynamically more favorable for the C−O−C group to adsorb there instead.

The final functional group considered is the COOH group. This species replaced one of the hydrogen atoms at the edge of the sheet and was orientated into four different configurations: two with the OH group 45° above the plane of the sheet, and two with the oxygen 45° above the plane of the sheet. There were two of each because for each case the hydrogen atom was placed to face either toward or away from the sheet. The Pt atom was placed into the three different edge locations where it would have the maximum ability to interact with the functional group that was above the plane of the sheet. Out of these 12 states, several duplicates were found, and out of the seven remaining configurations, the most stable with CO is shown in Figure 2a. The CO binding energy for this case is −2.43 eV. The lowest binding energy case calculated corresponds to when

dx.doi.org/10.1021/cm502447s | *Chem. Mater.* 2014, 26, 6142−6151

the −COOH group is rotated such that the hydroxyl points toward the Pt atom. Its calculated binding energy is −2.38 eV. The thermodynamic cost of this rotation versus the most stable configuration is 0.04 eV when no CO is present and 0.10 eV when CO is adsorbed onto the Pt, suggesting that −COOH may facilitate Pt nucleation on an edge in its vicinity and further facilitate reduced CO−Pt interactions.

Both the C−O−C and >C═O functional groups, seem to provide similar levels of resistance to CO interactions with the Pt. Even though the C−O−C system had a slightly smaller most stable binding energy configuration, its average, highest, and lowest binding energies are all larger than the >C═O values. This might be because there were more C−O−C systems considered over a more diverse range of the sheet. Some of the distances between the Pt and the C−O−C were quite large which would contribute to decreasing its effectiveness and raise the high and average CO binding energies. In the >C═O cases, the Pt was much more localized to the >C═O groups. Given that the ranges of the binding energies calculated and the most stable binding energies are similar, it is inconclusive which of the two functional groups inhibits CO adsorption onto a Pt atom more. They both seem to provide similar levels of resistance. It is important to note that in both of these cases, the most stable configuration is not one where the Pt adsorbs at edge sites that lead to the greatest decrease the CO−Pt binding energy, as calculated above in the reference calculations. In the C−O−C case, the CO−Pt binding energy after the removal of the functional group is −2.64 eV. In the >C═O case, the binding energy after the removal the functional group is −2.96 eV. There is a clear benefit when the functional group is present; however, it is apparently best for the Pt to be able to adsorb bridged over two carbon atoms on the edge of the sheet.

On the basis of these calculations, it can be concluded that the −COOH group provides the best route to improving this system's resistance to CO adsorption. The Pt does not need to compete with the −COOH functional group for available edge sites, unlike in the presence of C−O−C functional group. Furthermore, a thermodynamically low cost rotation of the moiety leads to an additional reduction in the binding energy. This is much more likely than, for example, the exchange of the Pt and C−O−C functional groups necessary to achieve any additional benefit oversimply having the Pt adsorbed on that edge site.

Table 1. Distances between Pt−C (in the Pt-CO) and the C−O Distance (in the CO) When Adsorbed onto the Pt in the Lowest Energy Configuration for Each Case

	distance (Å) in the presence of the oxygen species below				
bond	plain	O−H	>C═O	C−O−C	HO−C═O
Pt−C	1.82	2.00	1.84	1.84	1.86
C≡O	1.15	1.13	1.17	1.17	1.17

The relative dissociation energy of CO from Pt with a single GO functional group present (in descending order) is OH > >C═O ≈ C−O−C > COOH. Thus, the OH had the highest dissociation energy, whereas the presence of the other functional groups reduced the CO−Pt binding energy compared to the equivalent clean graphene sheet. The −COOH group led to the lowest dissociation energy making it much easier to relieve Pt of adsorbed CO when −COOH was available in the vicinity compared to any other oxygen groups. The CO binding energy to Pt in the most stable states are summarized in Table S1 along with the highest, lowest, and average of all states sampled. This provides a clear indication about where the most stable state fitted into all the calculated systems. Figure 3 shows the most stable binding energies

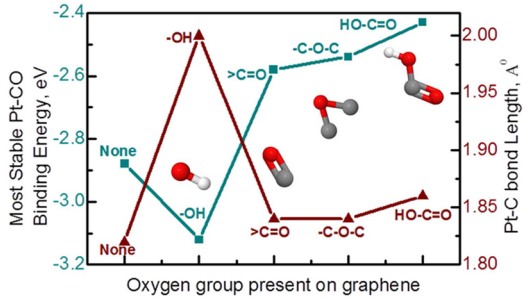

Figure 3. Most stable Pt−CO binding energy (eV) in the presence of the various oxygen groups and the variation in Pt−C bond length (Å), upon Pt−CO interaction in the presence of various oxygen groups.

observed along with the variation in the Pt−C bond length (Table 1) in the presence of the different oxygen groups.

CO-Stripping Studies for Pt/PR(GO−COOH). On the basis of the CO-stripping studies from Pt/PRGO and DFT calculations, further studies were carried out on samples with relatively more C═O groups (compared to C−O−C and C−OH) on GO. Single-bonded oxygen groups on GO were first converted to −COOH and >C═O (as described in the Experimental section of the Supporting Information) to obtain GO−COOH, which had 50% less C−O−C then GO. Pt nanoparticles where then grown on it using the MWAPP process (as described earlier in the Experimental section). The resultant Pt/PR(GO−COOH) had 3% more C═O groups (due to the conversion of less stable C−O−C groups) compared to Pt/PRGO. Table S2 compares the ratio of C−O to C═O components in Pt/PRGO and Pt/PR(GO−COOH) as obtained from XPS analysis. Pt loading in Pt/PR(GO−COOH) was similar to Pt/PRGO (TGA Figure S4), but the particle distribution (Figure 4a) seemed relatively less uniform, which may result from the decreased number of oxygen defect sites, acting as nucleation sites (due to the conversion of single bonded oxygen groups to double bonded oxygen groups which is evident in Table S3, as well as XPS graphs in Figures S2 and S3).

CO stripping at the Pt/PRGO−COOH samples was difficult to measure: several adsorption−stripping cycles were required before a well-defined peak in the current was obtained. Initial voltammograms displayed low current at relatively positive onset (an example is given in Figure 4c). Multiple CO oxidation and stripping cycles conducted on a single Pt/PRGO−COOH sample revealed a clear shift in the peak patterns and a slight shift of the onset potential to higher potentials, whereas the current intensity of the peak as well as area under the peak remained smaller (Figure 4b,c) than that of Pt/CB as well as Pt/PRGO. The progressive change in the peak pattern, intensity, and onset can be explained by changes in the surface functional groups upon successive potential cycling. The final stripping voltammogram exhibited a larger peak than those obtained for Pt/CB and Pt/PRGO samples, with a slightly more negative onset than for Pt/PRGO. This observation is in tandem with the DFT calculations, suggesting that the COOH group appears to provide the maximum resistance to CO adsorption among the four oxygen functional groups.

dx.doi.org/10.1021/cm502447s | Chem. Mater. 2014, 26, 6142−6151

The −COOH group may also have a tendency to break down into smaller oxygen moieties (because the rotation of the OH group in −COOH is thermodynamically favored as suggested by DFT studies), such that the presence of increased −COOH groups initially prevents CO adsorption on a large number of Pt sites leading to significantly lower CO adsorption for the same Pt loading. This would also explain the occurrence of low current intensity CO-oxidation peaks (Figure 4c) when CO

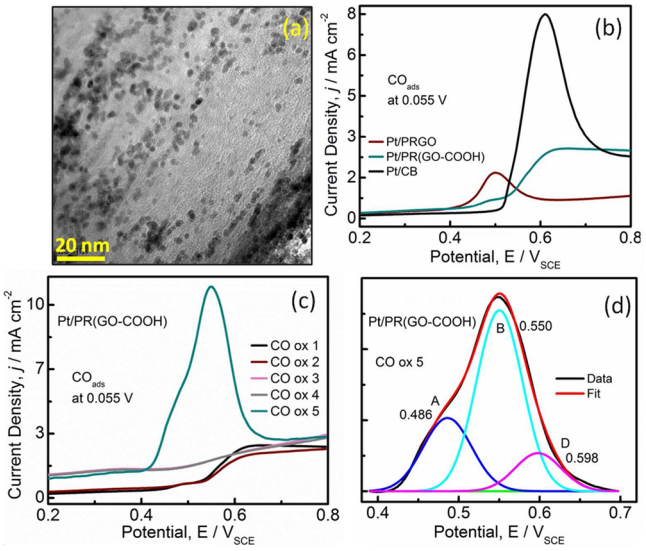

Figure 4. (a) TEM image of the Pt/PR(GO−COOH) sample; CO stripping on Pt/PR(GO−COOH) samples (b) compared to Pt/PRGO and Pt/CB samples; (c) upon multiple CO-stripping cycles; and (d) deconvolution of the CO-stripping voltammogram.

adsorption is carried out for the first few times on the same electrode. When the −COOH group breaks down to smaller oxygen groups (such as −OH, C═O, etc.), CO adsorption is able to take place at more sites (or newly exposed Pt (111) sites). The CO-stripping peaks observed as a result after multiple stripping cycles are at significantly more negative potentials (onset potential near 0.4 V and centered close to 0.5 V), similar to PRGO system, but a significantly higher CO-oxidation stripping current which is comparable to Pt/CB is also observed. Although the Pt/CB CO-stripping peak is normally centered at 0.6 V this peak from Pt/PR(GO−COOH) system tails off at 0.6 V and the contribution of the component D is significantly smaller compared to that in Pt/CB. The deconvolution of the CO-stripping peak hence observed is seen in Figure 4d, which revealed peaks A, B, and D at 0.48, 0.55, and 0.60 V, respectively.

In order to eliminate any possible contribution from the GO support, a CO-stripping study was also carried out on both PRGO and GO−COOH samples, and as expected, no CO-stripping peaks were observed.

Different Adsorption Potentials for Pt/PRGO. In order to study the effect of adsorption potential on specific oxygen groups, voltammograms were recorded for CO adsorption carried out at −0.25, −0.15 and 0.055 V The CO-stripping tests carried out after adsorption at these potentials revealed interesting patterns, suggesting that certain oxygen groups have preference toward interaction with approaching CO molecule at specific potentials.[49,50] Previous studies reported by Cuesta et al.[49] have confirmed the early onset of CO adsorption arising due to a competitive adsorption between H_2 and CO when CO is adsorbed at more negative potentials (within the H_{ads} region). As such, CO-stripping analysis after adsorption at these lower potentials would be helpful in understanding the Pt−CO interactions in the presence of the various residual oxygen groups. Because the results for 0.055 V have already been discussed in detail in the preceding sections, the following section focuses on the results for CO adsorption at −0.25 and −0.15 V in comparison with previous results. Scans conducted for Pt/CB samples for CO adsorbed at different potentials show only minor shifts, but the peak center largely remained close to 0.58−0.6 V.

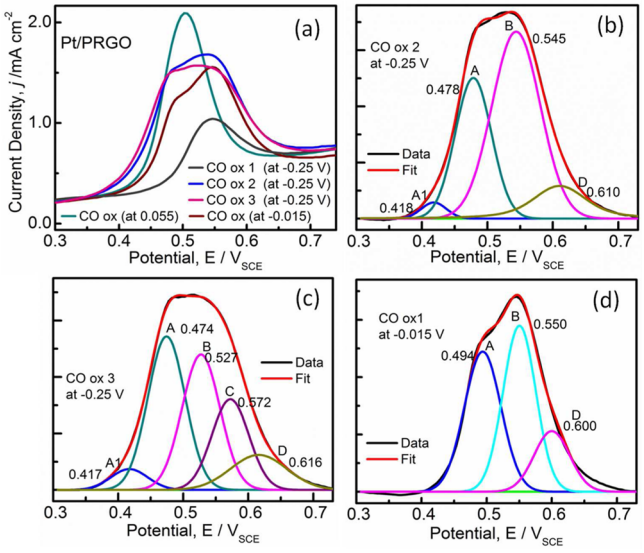

Figure 5. CO-stripping voltamogramms for Pt/PRGO (a) at different adsorption potentials; (b,c) deconvoluted at −0.25 V; (d) deconvoluted at −0.015 V.

Figure 5a shows the CO-stripping results after CO adsorption was carried out at different potentials for Pt/PRGO samples. Broad or shouldered peaks were clearly visible in the CO oxidation. The deconvolution of the peaks observed for samples with CO_{ads} potential at −0.25 V (Figure 5b,c) revealed four components at all times. Here again, the heterogeneous nature of the support seems to play a crucial role, and the contribution from each component varies depending on the particular local environment. However, a new component (named A1) could also be seen occasionally at even more negative potentials between 0.41 and 0.44 V. For these samples, the onset potential is also shifted toward more negative potential (i.e., ∼0.35 V compared to ∼0.4 V) for most Pt/PRGO samples. Interestingly, this peak is only seen in combination with peak A (i.e., A1 was never observed in the absence of A), although the reverse does not hold true. Previous reports suggest that Pt (111) orientations show CO-stripping peaks at potentials close to 0.6576 V vs SHE (i.e.0.4327 V vs SCE).[40] The fact that A1 was also observed at potentials lower than 0.42 V further confirms the DFT studies by Fampiou and Ramasubramaniam[28] that the strong Pt cluster−PRGO interaction can lower the cluster d-band center even below that of Pt (111).

Different Adsorption Potentials for Pt/PR(GO−COOH). Figure 6a shows three different CO-stripping data for Pt/PR(GO−COOH) samples after CO adsorption is carried out at −0.25 V. All scans revealed either a broad peak with a shoulder or a clear split in the stripping peak. This change in the nature of stripping peaks is suggestive of the differences in

dx.doi.org/10.1021/cm502447s | Chem. Mater. 2014, 26, 6142−6151

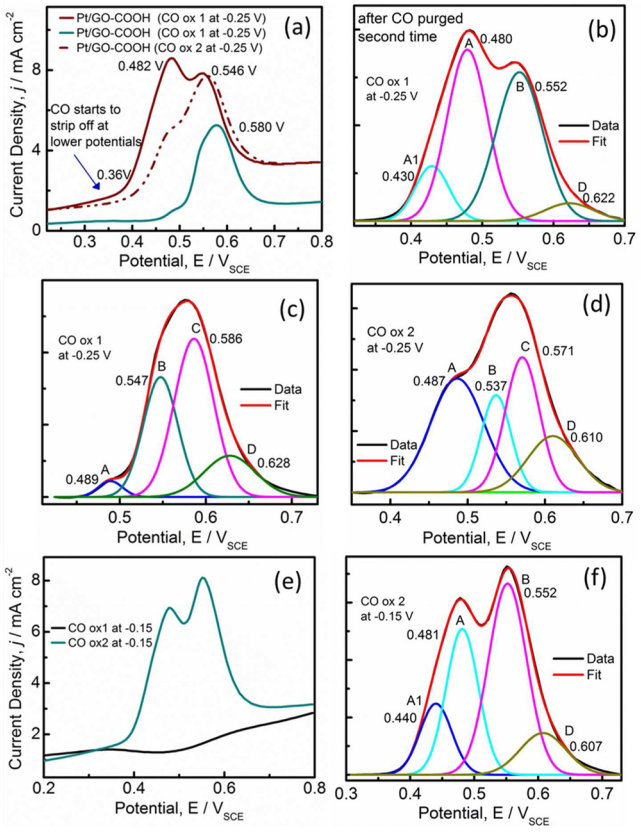

Figure 6. CO-stripping peaks for Pt/PR(GO−COOH) with CO adsorbed at (a) −0.25 V and (e) −0.15 V. Deconvoluted peak components obtained for CO adsorbed at (b−d) −0.25 V and (f) −0.15 V.

the structural composition of Pt/PR(GO−COOH), as compared to Pt/PRGO. The deconvolutions (Figure 6b−d) revealed the presence of at least four different components (A, B, C, and D) with variable contributions. Similar to Pt/PRGO, the component A1 was observed for CO adsorption at negative potentials. The fact that it was only observed when CO stripping was carried out the second time or more than few times on the same electrode and was observed in more instances for Pt/PR(GO−COOH) samples suggests a possible breakdown of −COOH into smaller functional groups, leading to exposure of the underlying Pt (111) site allowing CO oxidation to take place at more negative potentials. This clearly revealed the change in peak components after multiple stripping cycles and showed more similarity to the CO-stripping peak for Pt/PRGO.

It has to be emphasized at this point that the COOH is a large species with very specific spatial orientation, which may behave as a stearic hindrance between the Pt active site and the incoming CO, which also has very specific orientation. This further supports the DFT studies that −COOH provides maximum resistance toward CO adsorption compared to all other oxygen groups available on PRGO. However, the number of catalytic sites spatially hindered by the −COOH molecule is not expected to be very large, and this theory does not completely explain the relatively high CO-stripping current (comparable to Pt/CB) finally observed in the case of Pt/PR(GO−COOH). Figure 6e shows two CO-stripping scans obtained at −0.15 V for Pt/PR(GO−COOH). Figure 6f shows the deconvolution of the second peak obtained in the Pt/PR(GO−COOH) sample

Table 2. List of CO-Oxidation Peaks/Components Observed in This Work for GO-Based Electrocatalyst Systems: Pt/PRGO and Pt/PR(GO−COOH)—Their Suggested Attributions and Origins

peak position (V) vs SCE	attribution	remarks/observation	supporting reference
0.41−0.44 (A1)	Pt (111)	only observed in 2nd or higher number of CO-stripping cycles for Pt/PRGO and Pt/PR(GO−COOH)	28,40
		defects due to oxygen groups lead to strong Pt-binding traps enabling strong Pt−support interaction and hence downshift of Pt d-band centers	
0.47−0.49 (A)	interparticle oxidation and Pt (111)	observed and reported for high loading Pt/CB samples attributed to aggregation conditions	39
		in the case of Pt/PRGO and Pt/PR(GO−COOH) possibly facilitated by spatial orientation due to sheet folding and stretching due to functional oxygen groups in PRGO, giving rise to terrace-like features	28,40
		downshift of Pt d-band centers in PRGO and PR(GO−COOH)	
0.53−0.55 (B)	Pt in the presence of COOH	−COOH has the lowest dissociation energy in DFT studies	this work
		only observed in Pt/PRGO and Pt/PR(GO−COOH)	
		observed as a more consistent and strong component in Pt/PR(GO−COOH) especially at lower CO adsorption potential of −0.15 V	
0.57−0.59 (C)	Pt on carbon support Pt−PRGO and PR(GO−COOH) — C−O−C or >C═O	observed for 30−50 wt % Pt on carbon (in this study, the samples used were 46.9% Pt/CB)	39
		shifted to lower potentials by 10−20 mV in the presence of >C═O or C−O−C in Pt/PRGO, possibly due to the enhanced Pt−support interaction and decreased Pt−CO interaction energies	this work
0.61−0.63 (D)	Pt on carbon black support	observed in Pt/CB, Pt/PRGO, and Pt/PR(GO−COOH)	
		common and strong component in Pt/CB	39
		(SUGGESTED) Pt−carbon support interaction	
		relatively small and inconsistent component in Pt/PRGO and Pt/PR(GO−COOH)	

dx.doi.org/10.1021/cm502447s | Chem. Mater. 2014, 26, 6142−6151

when CO adsorption was performed at −0.15 V, revealing components similar to those observed for the −0.25 V case.

On the basis of the CO-striping peak analysis and the DFT studies, the observed peaks have been attributed to various factors discussed in this paper. Table 2 compiles all the peaks and their possible attributions based on the discussions in this paper and available literature.

CONCLUSIONS

In conclusion, we have carried out detailed CO-stripping analysis and DFT studies on Pt nanoparticle partially decorated reduced graphene oxide and carboxylated graphene oxide supports. CO-stripping studies carried out on Pt/PRGO and Pt/PR(GO−COOH) revealed multiple peaks and exclusive components upon further deconvolution. The role of COOH in enabling CO stripping is clearly visible from the CO-stripping peaks observed for CO adsorbed at lower potentials in the Hupd region and is further substantiated by DFT, which shows that the −COOH group provides Pt with the most resistance to CO adsorption. Furthermore, through XPS and TEM analysis, it was confirmed that although C−OH and C−O−C groups, abundant on the basal planes are responsible for the nucleation and distribution of Pt nanoparticle across the graphene sheets, the C═O groups (>C═O, −COOH) are more abundant residual species post Pt nanoparticle growth and play a vital role in enhancing CO tolerance of the Pt/PRGO and Pt/PR(GO−COOH) system. Further, DFT analysis on edge sites suggests that while CO−Pt interaction is reduced for Pt on edge sites, the presence of −COOH on the edge sites can favor/facilitate Pt nucleation on the edge/defect site and further reduce CO−Pt binding energy by a thermodynamically favorable rotation of the −OH group (of the −COOH group) toward the Pt. The authors appreciate that the geometric orientation of the approaching CO would certainly have a role to play in the CO−Pt interaction, especially since the Pt/PRGO surface also seems to offer various geometric configurations arising not only from the well-known heterogeneity in the structure of GO (due to randomly placed/reduced oxygen groups leading to generation of holes in the honeycomb structure and consequent new edge/defect sites) but also due to (i) the inhomogeneous C−C bond stretching in the parent graphene/honeycomb structure caused by the randomly attached oxygen groups and (ii) the folding and bending of the sheet which leads to heightened possibilities of step or terrace like features (similar to the model proposed by Lopez-Cudero et al.) enabling interparticle oxidation even with low loading Pt/PRGO systems. These features along with the various CO-oxidation potentials facilitated by the presence of multiple oxygen groups are expected to assist CO oxidation at much lower potentials in well-designed and tailored systems. Both the CO stripping and DFT analysis clearly suggest that tailoring the graphene oxide surface to increase the presence of carbonyl, carboxyl, and epoxides would certainly enable the synthesis of Pt supported on reduced graphene systems with significantly enhanced CO tolerance which may be comparable with that obtained with the use of other expensive oxophillic materials.

ASSOCIATED CONTENT

Supporting Information

XPS, XRD, TGA, and further details on the full cyclic voltammograms and DFT code are available in the Supporting Information. This material is available free of charge via the Internet at http://pubs.acs.org.

AUTHOR INFORMATION

Corresponding Author

*E-mail: s.sharma.1@bham.ac.uk.

Present Address

[¶]Department of Physics and Astronomy, Aarhus University, 8000 Aarhus C, Denmark.

Notes

The authors declare no competing financial interest.

ACKNOWLEDGMENTS

We are grateful to EPSRC (grant reference EP/K023853/1) for funding access to Nanoequipment facilities and expertise under the Leeds EPSRC Nanoscience Research Equipment Access Facility (LENNF) scheme. The X-ray photoelectron spectra were obtained at the National EPSRC XPS User's Service (NEXUS) at Newcastle University, an EPSRC Mid-Range Facility, and the authors are thankful for the same. The authors would also like to thank the National Science and Engineering Research Council of Canada for support through a CGS-D award.

REFERENCES

(1) Zhou, W.; Zhou, Z.; Song, S.; Li, W.; Sun, G.; Tsiakaras, P.; Xin, Q. *Appl. Catal., B* **2003**, *46*, 273−285.

(2) Xia, B. Y.; Ng, W. T.; Wu, H. B.; Wang, X.; Lou, X. W. D. *Angew. Chem.* **2012**, *124*, 7325−7328.

(3) Antolini, E.; Gonzalez, E. *J. Power Sources* **2010**, *195*, 3431−3450.

(4) Ehteshami, S. M. M.; Zhou, W.; Chan, S. *Int. J. Hydrogen Energy* **2013**, *38*, 188−196.

(5) Lamy, C.; Jaubert, T.; Baranton, S.; Coutanceau, C. *J. Power Sources* **2014**, *245*, 927−936.

(6) Cheng, X.; Shi, Z.; Glass, N.; Zhang, L.; Zhang, J.; Song, D.; Liu, Z.; Wang, H.; Shen, J. *J. Power Sources* **2007**, *165*, 739−756.

(7) Faur Ghenciu, A. *Curr. Opin. Solid State Mater. Sci.* **2002**, *6*, 389−399.

(8) Modibane, K.; Williams, M.; Lototskyy, M.; Davids, M.; Klochko, Y.; Pollet, B. *Int. J. Hydrogen Energy* **2013**, *38*, 9800−9810.

(9) Wang, C.; Li, B.; Lin, H.; Yuan, Y. *J. Power Sources* **2012**, *202*, 200−208.

(10) Porsgaard, S.; Ono, L. K.; Zeuthen, H.; Knudsen, J.; Schnadt, J.; Merte, L. R.; Chevallier, J.; Helveg, S.; Salmeron, M.; Wendt, S. *ChemPhysChem* **2013**, *14*, 1553−1557.

(11) Grunes, J.; Zhu, J.; Yang, M.; Somorjai, G. A. *Catal. Lett.* **2003**, *86*, 157−161.

(12) Yang, M.; Rioux, R.; Somorjai, G. *J. Catal.* **2006**, *237*, 255−266.

(13) Montano, M.; Salmeron, M.; Somorjai, G. A. *Surf. Sci.* **2006**, *600*, 1809−1816.

(14) Rioux, R. M.; Komor, R.; Song, H.; Hoefelmeyer, J. D.; Grass, M.; Niesz, K.; Yang, P.; Somorjai, G. A. *J. Catal.* **2008**, *254*, 1−11.

(15) Ren, H.; Humbert, M. P.; Menning, C. A.; Chen, J. G.; Shu, Y.; Singh, U. G.; Cheng, W. *Appl. Catal., A* **2010**, *375*, 303−309.

(16) Sharma, C.; Awasthi, R.; Singh, R. *Int. J. Hydrogen Energy* **2013**, *38*, 15388−15394.

(17) Yin, M.; Huang, Y.; Liang, L.; Liao, J.; Liu, C.; Xing, W. *Chem. Commun.* **2011**, *47*, 8172−8174.

(18) Abdelkareem, M. A.; Ito, Y.; Tsujiguchi, T.; Nakagawa, N. *ECS Trans.* **2013**, *50*, 1959−1967.

(19) Zhao, Y.; Zhan, L.; Tian, J.; Nie, S.; Ning, Z. *Electrochim. Acta* **2011**, *56*, 1967−1972.

(20) Sharma, S.; Ganguly, A.; Papakonstantinou, P.; Miao, X.; Li, M.; Hutchison, J. L.; Delichatsios, M.; Ukleja. *J. Phys. Chem. C* **2010**, *114*, 19459−19466.

(21) Li, Y.; Gao, W.; Ci, L.; Wang, C.; Ajayan, P. M. *Carbon* **2010**, *48*, 1124−1130.

(22) Antolini, E. *Appl. Catal., B* **2012**, *123*, 52−68.

(23) Nie, R.; Wang, J.; Wang, L.; Qin, Y.; Chen, P.; Hou, Z. *Carbon* **2012**, *50*, 586−596.
(24) Huang, C.; Pu, N.; Wang, C.; Huang, J.; Sung, Y.; Ger, M. *Sep. Purif. Technol.* **2011**, *82*, 210−215.
(25) Aboutalebi, S. H.; Aminorroaya-Yamini, S.; Nevirkovets, I.; Konstantinov, K.; Liu, H. K. *Adv. Energy Mater.* **2012**, *2*, 1439−1446.
(26) Kundu, P.; Nethravathi, C.; Deshpande, P. A.; Rajamathi, M.; Madras, G.; Ravishankar, N. *Chem. Mater.* **2011**, *23*, 2772−2780.
(27) Yoo, E. J.; Okata, T.; Akita, T.; Kohyama, M.; Nakamura, J.; Honma, I. *Nano Lett.* **2009**, *9*, 2255−2259.
(28) Fampiou, I.; Ramasubramaniam, A. *J. Phys. Chem. C* **2012**, *116*, 6543−6555.
(29) Groves, M. N.; Malardier-Jugroot, C.; Jugroot, M. *J. Phys. Chem. C* **2012**, *116*, 10548−10556.
(30) Lerf, A.; He, H.; Forster, M.; Klinowski, J. *J. Phys. Chem. B* **1998**, *102*, 4477−4482.
(31) Dreyer, D. R.; Park, S.; Bielawski, C. W.; Ruoff, R. S. *Chem. Soc. Rev.* **2010**, *39*, 228−240.
(32) Ganguly, A.; Sharma, S.; Papakonstantinou, P.; Hamilton, J. *J. Phys. Chem. C* **2011**, *115*, 17009−17019.
(33) Eda, G.; Fanchini, G.; Chhowalla, M. *Nat. Nanotechnol.* **2008**, *3*, 270−274.
(34) Du, D.; Wang, L.; Shao, Y.; Wang, J.; Engelhard, M. H.; Lin, Y. *Anal. Chem.* **2011**, *83*, 746−752.
(35) Bong, S.; Kim, Y. R.; Kim, I.; Woo, S.; Uhm, S.; Lee, J.; Kim, H. *Electrochem. Commun.* **2010**, *12*, 129−131.
(36) Sugimoto, W.; Aoyama, K.; Kawaguchi, T.; Murakami, Y.; Takasu, Y. *J. Electroanal. Chem.* **2005**, *576*, 215−221.
(37) Crabb, E.; Ravikumar, M.; Thompsett, D.; Hurford, M.; Rose, A.; Russell, A. *Phys. Chem. Chem. Phys.* **2004**, *6*, 1792−1798.
(38) Vidaković, T.; Christov, M.; Sundmacher, K.; Nagabhushana, K.; Fei, W.; Kinge, S.; Bönnemann, H. *Electrochim. Acta* **2007**, *52*, 2277−2284.
(39) López-Cudero, A.; Solla-Gullón, J.; Herrero, E.; Aldaz, A.; Feliu, J. M. *J. Electroanal. Chem.* **2010**, *644*, 117−126.
(40) Chen, Q.; Solla-Gullón, J.; Sun, S.; Feliu, J. M. *Electrochim. Acta* **2010**, *55*, 7982−7994.
(41) Lee, S. W.; Chen, S.; Sheng, W.; Yabuuchi, N.; Kim, Y.; Mitani, T.; Vescovo, E.; Shao-Horn, Y. *J. Am. Chem. Soc.* **2009**, *131*, 15669−15677.
(42) Li, J.; Kudin, K. N.; McAllister, M. J.; Prud'homme, R. K.; Aksay, I. A.; Car, R. *Phys. Rev. Lett.* **2006**, *96*, 176101.
(43) (a) Ertl, G.; Neumann, M.; Streit, K. M. *Surf. Sci.* **1977**, *64*, 393−410. (b) Winicur, D. H.; Hurst, J.; Becker, C. A.; Wharton, L. *Surf. Sci.* **1981**, *109*, 263−275. (c) Liao, M.-S.; Cabrera, C. R.; Ishikawa, Y. *Surf. Sci.* **2000**, *445*, 267−282. (d) Okamoto, Y. *Chem. Phys. Lett.* **2006**, *420*, 382−386.
(44) (a) Stamenkovic, V.; Schmidt, T.; Ross, P.; Markovic, N. *J. Phys. Chem. B* **2002**, *106*, 11970−11979. (b) Marković, N.; Ross, P., Jr *Surf. Sci. Rep.* **2002**, *45*, 117−229.
(45) Stamenkovic, V. R.; Fowler, B.; Mun, B. S.; Wang, G.; Ross, P. N.; Lucas, C. A.; Markovic, N. M. *Science* **2007**, *315*, 493−497.
(46) Lim, B.; Jiang, M.; Camargo, P. H.; Cho, E. C.; Tao, J.; Lu, X.; Zhu, Y.; Xia, Y. *Science* **2009**, *324*, 1302−1305.
(47) Mars, P.; Van Krevelen, D. W. *Chem. Eng. Sci.* **1954**, *3*, 41−59.
(48) Doornkamp, C.; Ponec, V. *J. Mol. Catal. A: Chem.* **2000**, *162*, 19−32.
(49) (a) Cuesta, A.; Couto, A.; Rincón, A.; Perez, M.; Lopez-Cudero, A.; Gutierrez, C. *J. Electroanal. Chem.* **2006**, *586*, 184−195;(b) *J. Electroanal. Chem.* **2005**, *579*, 1−12;(c) *J. Electroanal. Chem.* **2006**, *586*, 204−216.
(50) Vidaković, T.; Christov, M.; Sundmacher, K. *Electrochim. Acta* **2007**, *52*, 5606−5613.